Proceedings of the SPIE Smart Structures Conference, Vol. 4695, Paper No. 35., San Diego, CA., March 2002,

The use of Piezoelectric Resonators for the Characterization of Mechanical Properties of Polymers

S. Sherrit, V. Olazábal, J.M. Sansiñena, X. Bao, Z. Chang, Y. Bar-Cohen
Jet Propulsion Laboratory, Caltech, Pasadena, CA

ABSTRACT

In this paper a variety of techniques to characterize the mechanical properties of polymers in the MHz frequency range based on the impedance analysis of thickness and thickness shear composite resonators will be presented. The analysis is based on inverting the impedance data of the composite resonator to find the best fit using the material coefficients of the piezoelectric resonator and attached polymer layer. Mason's equivalent circuit is used along with standard acoustic circuit elements to generate the impedance of the composite resonators and interpret the experimental data. Inversion techniques will be presented which allow for the direct determination of the acoustic load if the material properties of the resonator are known before being joined to the polymer.

A specific example of this technique, the quartz crystal microbalance will be presented and it will be shown how the model can be extended to include all the acoustic elements of the experimental setup including the acoustic load of the solution. In the model all elements are treated as complex to account for loss mechanisms (viscous effects, electric dissipation etc.). If the free resonator is modeled prior to deposition a transform is presented that allows for the determination of the acoustic load directly. The advantage being that one no longer has to assume a functional form of the acoustic load (eg. mass damping) since it can be measured directly and compared to the various models. In addition the transform allows for an easy determination of the mass sensitivity and bandwidth for the system. The theory can be extended to account for electrode mass changes (adsorption/condensation and desertion/evaporation) or for use in chemical monitoring by the addition of a chemically sensitive layer (artificial noses and tongues). The technique has also applications for the direct determination of the elastic coefficients of polymer materials.

Keywords: Piezoelectric devices, Active Materials, Thin Film Resonators, Composite Resonators, Quartz Crystal Microbalance.

1. INTRODUCTION

Analytical solutions to the wave equation in piezoelectric materials can be quite cumbersome to derive from first principles in all but a few cases. Mason[1,2] was able to show that for one-dimensional analysis most of the difficulties in deriving the solutions could be overcome by borrowing from network theory. He presented an exact equivalent circuit that separated the piezoelectric material into an electrical port and two acoustic ports through the use of an ideal electromechanical transformer as shown in Figure 1. The model has been widely used for free and mass loaded resonators[3], transient response[4], material coefficient determination[5], and a host of other applications[6]. One of the perceived problems with the model is that it required a negative capacitance at the electrical port. Although Redwood[4] showed that this capacitance could be transformed to the acoustic side of the transformer and treated like a length of the acoustic line it was still thought to be "un-physical". In an effort to remove circuit elements between the top of the transformer and the node of the acoustic transmission line Krimholtz, Leedom and Matthae[7] published an alternative equivalent circuit as shown in Figure 1. The model is commonly referred to as the KLM model and has been used extensively in the medical imaging community in an effort to design high frequency transducers [8,9,] multilayers[10], and arrays[11]. In a recent paper[12] we presented results, which extended both models to include loss components in all the material coefficients, and demonstrated that if losses were treated consistently both the KLM and Mason's equivalent circuit produced identical impedance spectra. In the remaining sections of this paper we will be using the Mason's equivalent circuit exclusively. The Mason's equivalent circuit is shown in Figure 1 for the thickness/thickness shear mode. If the acoustic ports are shorted these models reduce to the free resonator equation derived from the linear piezoelectric equations and the wave equation[3] which has been adopted by the IEEE Standard on Piezoelectricity[13] for determination of the thickness material coefficients.

2. MASON'S NETWORK EQUIVALENT CIRCUIT

The constants of the Mason network equivalent model are shown in Table 1. In the circuit an electrical port is connected to the center node of the two acoustic ports representing the front and back faces of the transducer. On the electrical side of the transformer all circuit elements are standard electrical elements and the voltage is related to the current

via V =ZI where Z is an electrical impedance. On the acoustical side of the transformer the force F and the velocity v are related through $F = Z_a v$ where Z_a is the specific acoustic impedance $Z_a \propto \rho v A$ where ρ is the density, v is the longitudinal velocity of the piezoelectric material and A is the area. It should be noted that the italic $v = \partial u/\partial t$ is a variable of the circuit model while the straight v is a coefficient of the material. The transformer is an ideal electromechanical transformer that conserves power during the transformation. The relationship between the coefficients of the free resonator and Mason's equivalent circuits are shown in Table 1 in terms of the material coefficients of the free resonator.

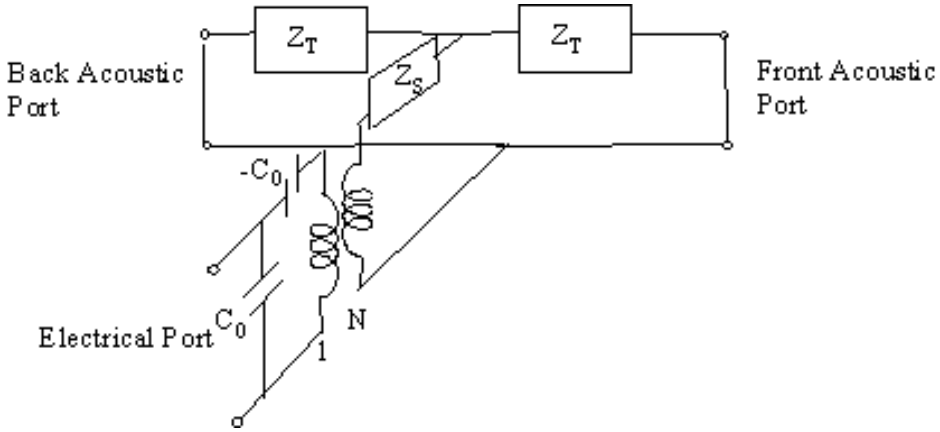

FIGURE 1: Mason's equivalent circuits with short circuits on the acoustic ports (unclamped). Quantities in figure are defined in Table 1.

Table 1. The complex material coefficients of Mason's equivalent circuit parameters and the equation and coefficients of the free resonator. The equations shown can be used to describe the thickness extensional and the thickness shear resonance mode.

Free Resonator
$\mathbf{Z} = \frac{t}{i\omega A \boldsymbol{\varepsilon}^S}\left(1 - \frac{\mathbf{k}^2 \tan\left(\frac{t\omega}{2}\sqrt{\frac{\rho}{\mathbf{c}^D}}\right)}{\frac{t\omega}{2}\sqrt{\frac{\rho}{\mathbf{c}^D}}}\right)$
$\boldsymbol{\varepsilon}^S$ clamped complex permittivity
$\mathbf{c}^D$ open circuit complex elastic stiffness
$\boldsymbol{k}$ complex electromechanical coupling
$\boldsymbol{k}^2 = \boldsymbol{e}^2/\mathbf{c}^D\boldsymbol{\varepsilon}^S = \boldsymbol{h}^2\boldsymbol{\varepsilon}^S/\mathbf{c}^D$
$\boldsymbol{h} = \boldsymbol{k}\sqrt{\mathbf{c}^D/\boldsymbol{\varepsilon}^S}$
Mason's Model
$\mathbf{C}_0 = \frac{\boldsymbol{\varepsilon}^S A}{t}$ $\quad$ $\mathbf{N} = \mathbf{C}_0\boldsymbol{h}$
$\boldsymbol{Z}_0 = \rho A\mathbf{v}^D = A\sqrt{\rho\,\mathbf{c}^D}$ $\quad$ $\boldsymbol{\Gamma} = \frac{\omega}{\mathbf{v}^D} = \omega\sqrt{\frac{\rho}{\boldsymbol{c}^D}}$
$Z_T = i\mathbf{Z}_0\tan(\boldsymbol{\Gamma}t/2)$ $\quad$ $Z_S = -i\mathbf{Z}_0\csc(\boldsymbol{\Gamma}t)$

In the small signal limit the material loss of linear systems can be accurately described by the use of complex coefficients[14]. A variety of techniques to determine these complex coefficients have been published previously [15,16,17, 18]. In the case of the thickness extensional/ thickness shear resonator the material coefficients can be represented by

$$\varepsilon^S = \varepsilon_r^S + i\varepsilon_i^S = \varepsilon_r^S(1 + i\tan\delta_E) \tag{1}$$

$$c^D = c_r^D + ic_i^D = c_r^D(1 + i\tan\delta_M) \tag{2}$$

$$h = h_r + ih_i = h_r(1 + i\tan\delta_P) \tag{3}$$

where it should be noted that we have not imposed any sign on the imaginary component in equations 1 to 3. It should also be noted that representation is a simplification that is theoretically only exact at a single frequency due to the possibility of dispersion in each of the material coefficients. As an example consider the general case of an elastic media with viscous losses. The stress T is

$$T = cS + \eta \dot{S} \tag{4}$$

For a harmonic strain $S=\mathrm{Re}(S_0 e^{i\omega t})$ the stress can be rewritten as

$$T = (c + i\omega\eta)S = \mathbf{c}S \tag{5}$$

In the case of most solid materials it has been point out by Mason[19] that the imaginary term in the brackets in equation 5 (loss component) is frequency independent which implies at least for many solid materials that η has an inverse frequency dependence. The complex coefficient representation is generally valid unless the frequency of operation happens to coincide with an anomalous adsorption/relaxation peak in the material coefficient since away from these peaks the frequency dependence is generally quite small. The shear velocity $\boldsymbol{v}$ described in the equations for the acoustic impedance Z_0 and propagation constant Γ is therefore complex and can be determine from the complex shear stiffness coefficient using

$$\mathbf{v} = \sqrt{\frac{\mathbf{c}^D}{\rho}} \tag{6}$$

Similar dispersion relationships may hold for the permittivity and the piezoelectric coefficient[14] which over a limited bandwidth may be treated as a complex coefficient.

In the case of the free thickness extensional or thickness shear resonator the electrical impedance determined from Mason's equivalent circuit $\mathbf{Z}_M$ measured at the electrical port is

$$\mathbf{Z}_M = \mathbf{Z}_C\left(1 - \frac{\mathbf{Z}_C\mathbf{N}^2}{\mathbf{Z}_A}\right) \tag{7}$$

with

$$\mathbf{Z}_A = \mathbf{Z}_S + \frac{\mathbf{Z}_T}{2} \tag{8}$$

and

$$\mathbf{Z}_C = \frac{1}{i\omega\mathbf{C}_O} \tag{9}$$

with the functions $\mathbf{Z}_T$ and $\mathbf{Z}_S$ and the complex capacitance $\mathbf{C}_O$ defined in Table 1. The impedance equation $\mathbf{Z}_M$ shown in equation 7 can be shown to be identical to the equation for the free resonator shown in Table 1 as would be expected.

3. ACOUSTIC ELEMENTS

In order to investigate the various acoustic regimes encountered when a layer is attached to a surface of a piezoelectric we use the network representation of a non-piezoelectric solid acoustic element as described by Redwood[4] and McSkimmin[20]. This network representation is shown in Figure 2. Like Mason's model this representation is the solution to the one-dimensional wave equation with open boundary conditions.

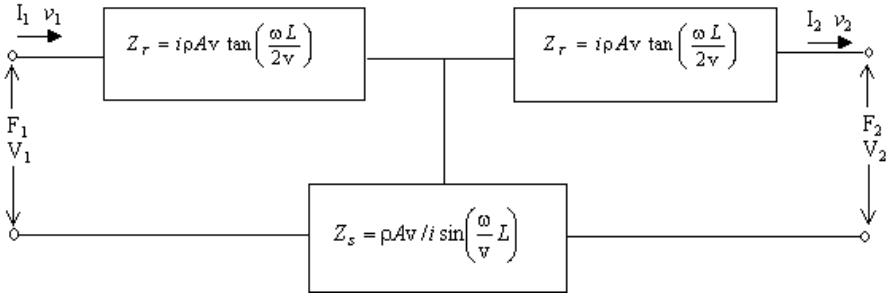

Figure 2. Network representation of the one-dimensional solution to the wave equation for an extensional mode in a plate. The boundary conditions are open. Electrical Analogs are Voltage = Force, Current = Velocity and Specific acoustic impedance is analogous to the electrical impedance. Losses can be accounted for by allowing the velocity to be complex $v^*=(c^*/\rho)^{1/2}$.

In order to emphasize the versatility of this representation we have investigated the response of this layer network in the low and high frequency regimes when the front face of the layer is acoustically short circuited (free to expand) and open circuited (rigidly clamped). The back surface is driven by a sinusoidal force $F=F_o\cos(\omega t)$. For harmonic sinusoidal excitation in a linear system the displacement u_1 of the back face is related to the velocity v_1 by $v_1=i\omega u_1$. The acoustic impedance of the layer under open and short circuit conditions is

$$Z_{Open} = Z_T + Z_S \tag{10}$$

$$Z_{Short} = Z_T + \frac{Z_T Z_S}{Z_T + Z_S} \tag{11}$$

At high frequencies the acoustic element goes into resonance. The elastic properties, geometry and boundary conditions determine the resonance frequency. In the case where one face of the element is rigidly fixed (open circuit) the resonance frequency in determined from the minimum of Z_{Open} and the plate is found to resonate at $\lambda/4$. When the acoustic port is short-circuited the acoustic impedance of the element can be shown to equal $Z_{short}= iZ_b\tan(\omega L/v)$ and is found to resonate at $\lambda/2$. The frequency response (derived from equations 10 and 11) of the logarithm of the longitudinal velocity v is shown in Figure 3 for both the open and short circuit acoustic ports. The coefficients used for this simulation are shown in the figure caption. In this case we assume a thickness extensional excitation.

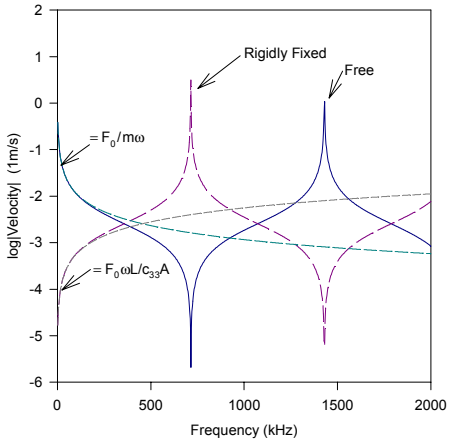

Figure 3. The velocity of the front face of an acoustic element being driven by a sinusoidal force when the back face of the acoustic port is a) free and b) rigidly fixed.. (A= 0.0025 m^2, L =0.002 m, ρ = 2750 kg/m^3, v=(5721+2.86i) m/s, F_0 = 100 N, m =0.01375 kg, and $c_{33} = 9x10^{10}$ (1+0.001i)).

In the low frequency limit as $\omega\rightarrow 0$ the tan function $\tan(\omega L/2v) \rightarrow \omega L/2v$ while the $\sin(\omega L/v) \rightarrow \omega L/v$. The acoustic impedance of each element reduces to $Z_T \rightarrow i\rho A\omega L/2 = im\omega/2$, $Z_S \rightarrow \rho A v^2/i\omega L = Ac_{33}/i\omega L$ where m is the mass of the layer and c_{33} is the elastic stiffness. In the case where the front surface is rigidly fixed we note that at low frequencies $Z_S >> Z_T$

$$Z_{Open} = Z_S = Ac_{33}/i\omega L \tag{12}$$

and the total impedance appears capacitive with a capacitance $C = L/Ac_{33}$. The strain $S = u_1/L$ for a sinusoidal force $F_1 = F_0\cos(\omega t)$ is therefore

$$S = \frac{u_1}{L} = \frac{F}{i\omega L Z_{Open}} = -\frac{1}{c_{33}}\frac{F_0}{A}\cos(\omega t) \tag{13}$$

This is the equation of an elastic solid being strained (Hooke's Law) by the application of a sinusoidal force, which is exactly what one would expect.

In the case where the layer is short-circuited the total impedance at low frequency is

$$Z_{Short} = 2Z_T = im\omega \tag{14}$$

and the impedance is inductive with an inductance L = m the mass of the acoustic layer. The displacements of the front and back faces u_1, u_2 are found to be

$$u_2 = u_1 = -\frac{1}{m}\frac{F_0}{\omega^2}\cos(\omega t) \tag{16}$$

which is the equation for a displacement of a mass driven by a harmonic force.

4. LAYER MODELING

The analytical solution for the impedance of a piezoelectric layer on a substrate was derived from the wave equation by Lakin, Kline and McCarron[21]. A more recent derivation by Lukacs et al[22] extended the solution to include loss in the elastic, dielectric and piezoelectric constants and first order dispersion in the dielectric constant. These models produced identical impedance spectra to the spectra generated using Mason's equivalent circuit shown in Figure 1. when loss was applied consistently[12]. These solutions are valid for all cases where the lateral dimensions of the acoustic layer and the piezoelectric layer are much larger than either layer thickness. In order to proceed with the modeling we connect one of the accoustic ports of Mason's equivalent circuit to one of the acoustic ports of an acoustic element and short the other acoustic port of the piezoelectric and acoustic element as is shown in Figure 4.

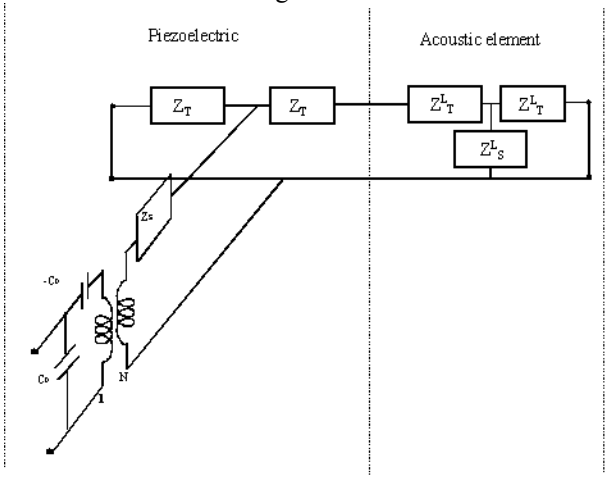

Figure 4. The equivalent circuit representation of the piezoelectric resonator attached to an acoustic element. The mechanical boundary conditions on both exposed surfaces of the element and piezoelectric are unclamped (short circuit on the acoustic port)

The acoustic elements of the layer are:

$$\mathbf{Z}_T^L = i\rho_l A_l \mathbf{v}_l \tan\left(\frac{\omega L}{2\mathbf{v}_l}\right) \tag{17}$$

$$\mathbf{Z}_S^L = \rho_l A_l \mathbf{v}_l / i\sin\left(\frac{\omega}{\mathbf{v}_l} L\right) \tag{18}$$

where ρ, A_l, $\mathbf{v}_l$ and L are the density, cross sectional area, complex velocity, and the thickness of the layer respectively. The elements of the layer shown in Figure 5 can be simplified further to give the total impedance of the layer $\mathbf{Z}_L$

$$\mathbf{Z}_L = \mathbf{Z}_T^L + \frac{\mathbf{Z}_T^L \mathbf{Z}_S^L}{\mathbf{Z}_T^L + \mathbf{Z}_S^L} = i\rho_l A_l \mathbf{v}_l \tan\left(\frac{\omega L}{\mathbf{v}_l}\right) \tag{19}$$

The electrical impedance of the piezoelectric and the layer determined from Mason's equivalent circuit is calculated using equation 7 with total acoustic impedance $\mathbf{Z}_A$ equal to

$$\mathbf{Z}_A = \mathbf{Z}_S + \frac{\mathbf{Z}_T(\mathbf{Z}_T + \mathbf{Z}_L)}{2\mathbf{Z}_T + \mathbf{Z}_L} \tag{20}$$

and $\mathbf{Z}_C$ defined as in equation 9. It can be shown that as the layer increases in thickness three distinct acoustic regions can be determined in which the total impedance of the layer $\mathbf{Z}_L$ has distinct and measurable effects on the resonance spectrum of the transducer. These regions are the mass, intermediate and radiation damping regions. In order to demonstrate these regimes the piezoelectric with an acoustic layer of various thickness values was simulated using the data in Tables 2 to 3. The graphs are shown in Figures 5 to 7.

Table 2. The complex material coefficients (nominal) used to investigate the resonator configurations. The coefficients for AT quartz were used to simulate the curves shown in Figures 5-9.

	AT Cut Quartz Thickness Shear Extensional
$\boldsymbol{\varepsilon}^S$ (F/m)	$5.30\text{x}10^{-11}(1 - 0.002i)$
$\mathbf{c}^D$ (N/m^2)	$2.94\text{x}10^{10}(1 + 4.5\text{x}10^{-6}i)$
$\boldsymbol{k}$ (#)	$0.071(1 - 0.001i)$
$\boldsymbol{h}$ (V/m)	$1.67\text{x}10^{9}(1 + 2.9\text{x}10^{-5}\ i)$
ρ (kg/m^3)	2650

Table 3. The complex elastic stiffness constant, density and thickness values used to generate the curves shown in Figures 5-9.

	Layer Properties
c (N/m^2)	$8\text{x}10^{10}(1+0.01i)$
ρ (kg/m^3)	2700
a) t (m)	0.00001
b) t (m)	0.003
c) t (m)	1

a) Mass Damping ($t/v^D >> L/v_l$)

In this region the layer thickness is much smaller than the piezoelectric thickness and the tan of the argument of the tan function of $\mathbf{Z}_L$ can be approximated by the argument (for x<<1 tan(x)≈x)

$$\mathbf{Z}_L = i\rho_l A_l \mathbf{v}_l \tan\left(\frac{\omega L}{\mathbf{v}_l}\right) = i\rho_l A_l \mathbf{v}_l \left(\frac{\omega L}{\mathbf{v}_l}\right) = im\omega \tag{21}$$

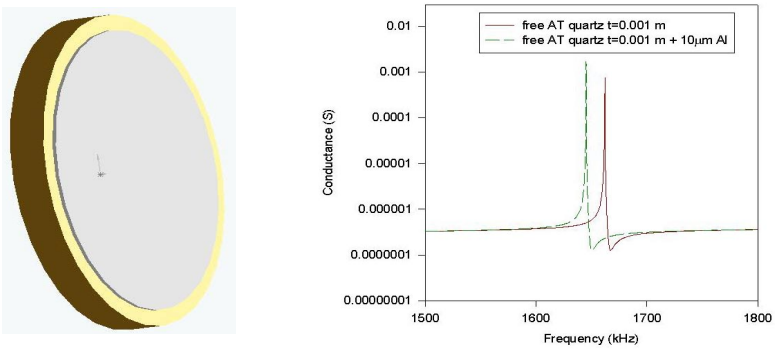

Figure 5 Schematic of a piezoelectric with a thin layer and the effect on the resonance spectra. The mass loads the piezoelectric and the resonance frequency shifts down. Layer thickness is not to scale.

As mass is deposited on the surface of the crystal the resonance frequency of the crystal is reduced. In the case of a thin rigid film deposited in vacuum deposition the shift Δf_s in resonance frequency f_s can be related to the deposited mass Δm by the Sauerbrey equation[23]. The quantity m_o is the mass of the crystal/electrodes in the active area of the resonator prior to deposition.

$$\Delta m = m_0 \frac{\Delta f_s}{f_s} \tag{22}$$

By monitoring the change in frequency one can then determine the change of the mass deposited on the surface of the resonator. In the example above in Figure 5 $\Delta f/f = \Delta m/m_0 = 0.0101$

A variety of models have been used to model the unloaded resonator about resonance. The most common is the Butterworth Van Dyke model[25]. In this lumped circuit model the loss around resonance is assumed to be dominated by mechanical effects and is accounted for by a resistor in the motional branch. In previous work[24] it was demonstrated that by removing the resistor and allowing the remaining circuit constants to have a complex component one could obtain a better fit to the resonator over a larger bandwidth. Although the lumped circuit models[25] applied to the Quartz Crystal Microbalance are attractive from an ease of use perspective they suffer limitations from the fact that they are approximations to the full one-dimensional solution of the resonator and film. In addition one needs to assume a model for the load on the acoustic port, which requires the addition of general capacitive, inductive and resistive impedance elements to be added to the motional branch. Although these electrical elements can in most cases account for the frequency shift and decrease in mechanical Q of the resonator film combination they lack a clear link to the physical process that is occurring at the surface of the quartz resonator.

A more elegant and rigorous (exact solution to the one-dimensional wave equation for the system) approach is to treat the resonator and film using multi-port network solutions as discussed above and described by Cernosek et. al.[26].

Mason's equivalents circuits can represent the solution to the one dimension wave equation for the system shown in Figure 4. The circuits are exact solutions to the wave equations for each region. Connecting each of the circuit elements allows for the matching of the mechanical boundary conditions at each interface. This representation is a powerful tool to solve the wave equation in piezoelectric and non-piezoelectric media especially when losses are properly accounted for.

b) Intermediate region ($t_P/v^D \approx L/v_l$)

In this regime approximations are not valid and the layer specific acoustic impedance is

$$\mathbf{Z}_L = i\rho_l A_l \mathbf{v}_l \tan\left(\frac{\omega L}{\mathbf{v}_l}\right) \tag{23}$$

Resonances in the layer are clearly present in the admittance curves

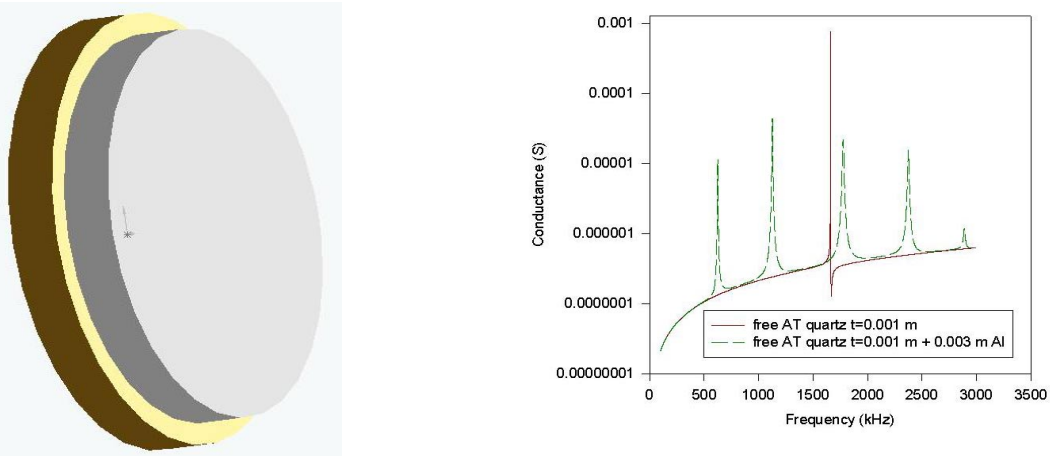

Figure 6 Schematic of a piezoelectric with a layer of approximately the same acoustic length. The effect on the resonance admittance spectra is shown in the curve. Multiple resonance peaks are now apparent. Layer thickness is not to scale.

c) Radiation limit ($t_p/v^D << L/v_l$)

In this region the piezoelectric is radiating mechanical energy into the layer, which due to the layer length and attenuation is not reflected back to the piezoelectric. With the assumption that attenuation is present it can be shown that $\tan(\mathbf{k}x) \rightarrow i$ as $x \rightarrow \infty$ where x is a real number and $\mathbf{k}$= a+ib is complex and b>0. If b<0 then $\tan(\mathbf{k}x) \rightarrow -i$. Therefore in the radiation limit for x large

$$\mathbf{Z}_L = i\rho_l A_l \mathbf{v}_l \tan\left(\frac{\omega L}{\mathbf{v}_l}\right) = i\rho_l A_l \mathbf{v}_l (-i) = \rho_l A_l \mathbf{v}_l \tag{24}$$

which is the specific acoustic impedance of the layer. It should be noted that in the case of a long rod that dispersion is present and the wave velocity will switch from being controlled by the compliance to the stiffness as the frequency is increased.

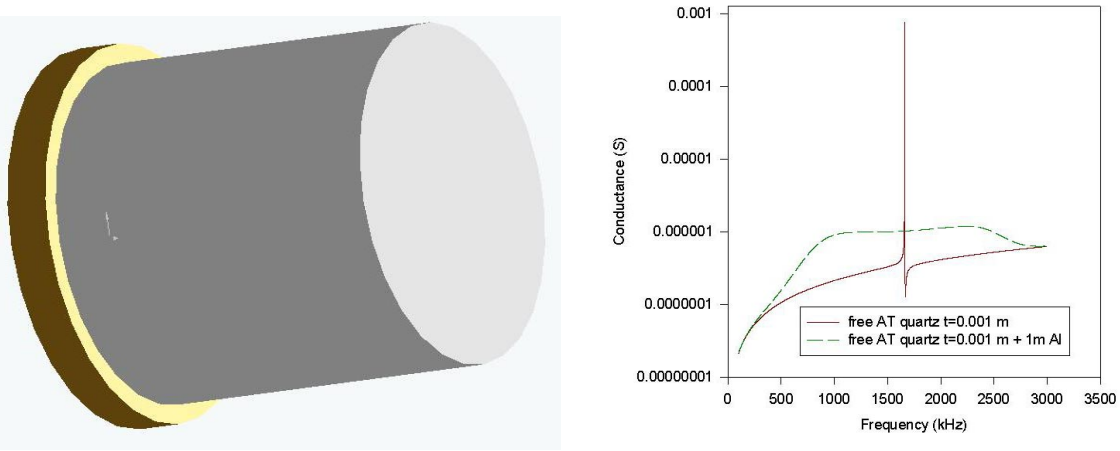

Figure 7 Schematic of a piezoelectric with a very thick layer and the effect on the resonance spectra. The radiation of energy reduces significantly the quality of the resonance. Layer thickness is not to scale.

The analysis suggests that in the first regime the mass of the layer (m) can be determined however restrictions to this are discussed below. In the second regime the velocity of the layer (v) can be determined while in the radiation limit one can determine the specific acoustic impedance (ρAv). If the density is known the elastic constant for the layer can be determined through $c = \rho v^2$ since A is the transducer electrode area in contact with the layer and is in general known.

5. DETERMININATION OF THE LAYER IMPEDANCE USING IMPEDANCE TRANSFORMS

Regardless of the loading of the layer and using Figure 4 the layer impedance $\boldsymbol{Z}_L$ can be determine directly from the turns ration $\boldsymbol{N}$, the total mechanical impedance $\boldsymbol{Z}_A$, the total electrical impedance of the composite $\boldsymbol{Z}$, and the impedance of the static capacitance $\boldsymbol{Z}_C$ and the two acoustic impedance elements of the piezoelectric $\boldsymbol{Z}_T$ and $\boldsymbol{Z}_S$ from

$$\mathbf{Z}_L = \frac{\mathbf{Z}_T^2 - 2\mathbf{Z}_T(\mathbf{Z}_A - \mathbf{Z}_S)}{\mathbf{Z}_A - \mathbf{Z}_S - \mathbf{Z}_T} \tag{25}$$

where

$$\mathbf{Z}_A = \frac{\mathbf{Z}_C \mathbf{N}^2}{\left(1 - \frac{\mathbf{Z}}{\mathbf{Z}_C}\right)} \tag{26}$$

Since $\boldsymbol{N}$, $\boldsymbol{Z}_C$, $\boldsymbol{Z}_T$, $\boldsymbol{Z}_S$ are known or can be determined from the free resonator and $\boldsymbol{Z}$ is measured on the composite resonator it is simply a matter of substituting the various spectra or coefficients into equations 25 and 26 to determine $\boldsymbol{Z}_L$. The acoustic impedance of the layer determined from equation 25 assumes that parasitic electrical impedance for the free resonator and the resonator and layer are identical. Typically quartz resonators have free capacitance values of the order of 10 pF and parasitic impedance, which can be as high as 1 pF. In addition the parasitic impedance can change depending on the orientation of the

sample or holder leads[27]. Also the addition of a layer on the piezoelectric operating in the thickness extensional mode can clamp the lateral motion in the piezoelectric changing the response of the piezoelectric from its free response. The solution to $\mathbf{Z}_L$ represented by equation 25 assumes no change in the mechanical and electrical boundary conditions. As an example we have taken the thickness shear spectra shown in Figure 5 and applied the transform. The results are shown in Figure 8 in terms of the real and imaginary components of $\mathbf{Z}_L$ and $\mathbf{m}^* = \mathbf{Z}_L/i\omega$. The layer mass calculated from $m=\rho AL$ = 8.48 mg and from the Sauerbrey equation m = 8.42 mg. The mass determined from the data in Figure 8 is m = 8.48 mg.

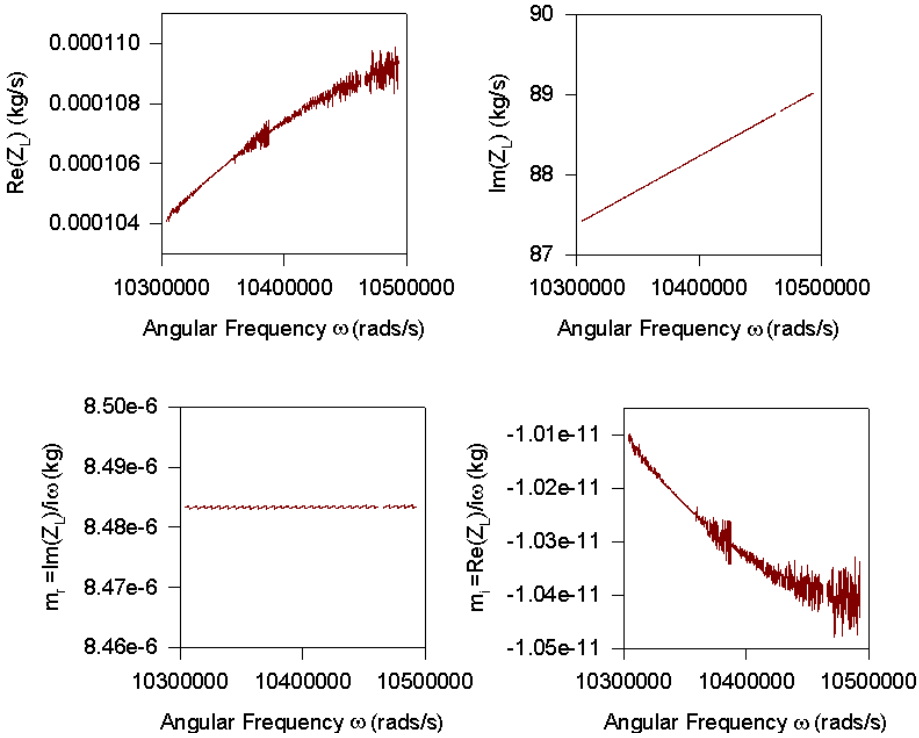

Figure 8 The complex acoustic impedance spectra of the layer as a function of the angular frequency determine from the data in Figure 5 and the transform shown in equation 25. The mass spectra of the layer determined from $\mathbf{Z}_L/i\omega$. Both the real and imaginary mass determined from the figure are in agreement with the theoretical complex mass.

The transform in equation 25 has both a real and imaginary component for the acoustic impedance and hence the mass. This can be explained if we expand the acoustic load.

$$Z_L = i\rho A v \tan\left(\frac{\omega L}{v}\right) \tag{27}$$

in terms of $x = \omega L/v$ and use $m = \rho LA$ to get

$$Z_L = im\omega\frac{\tan(x)}{x} \tag{28}$$

In the small x limit we can expand the tangent about x=0 to get

$$Z_L = im\omega\left[1+\frac{1}{3}x^2+\frac{2}{15}x^4\ldots\right] \tag{29}$$

Keeping only terms of second order in x and substituting the velocity dependence we find

$$Z_L = im\omega\left[1+\frac{1}{3}\frac{\omega^2 L^2}{v^2}\right] \tag{30}$$

which can be rewritten in terms of the complex elastic stiffness $\mathbf{c} = \rho v^2 = c_r + ic_i$ and using $m = \rho LA$ to finally get

$$\mathbf{Z}_L = im\omega\left[1+\frac{1}{3}\frac{\omega^2 m^2}{\rho A^2 \mathbf{c}}\right] = \frac{1}{3}\frac{\omega^3 m^3}{\rho A^2}\frac{c_i}{|\mathbf{c}|^2} + im\omega\left[1+\frac{1}{3}\frac{\omega^2 m^2}{\rho A^2}\frac{c_r}{|\mathbf{c}|^2}\right] \tag{31}$$

Dividing equation 31 by iω we finally arrive at the theoretical mass spectra for a thin film

$$\mathbf{m}^* = \left[m+\frac{1}{3}\frac{\omega^2 m^3}{\rho A^2}\frac{c_r}{|\mathbf{c}|^2}\right] - i\frac{1}{3}\frac{\omega^2 m^3}{\rho A^2}\frac{c_i}{|\mathbf{c}|^2} \tag{32}$$

The acoustic impedance associated with the mass is seen to have a correction term that is proportional to the real part of the elastic stiffness while the real component of the acoustic layer and the imaginary component of mass spectra $\mathbf{m}^* = \mathbf{Z}_L/i\omega$ is found to be controlled by the imaginary component of the stiffness. The mass from the slope of Im($\mathbf{Z}_L$) vs ω in Figure 8 is found to be 8.48 mg which is in agreement with the theoretical value. The imaginary part of the mass (-1.02×10^{-11}) determined from equation 31 and the constants of Table 3 are in general agreement with the value determined from the imaginary part of the mass spectra. It is clear from this second order expansion that the frequency shift that is measured using the Sauerbrey equation is due to the mass of the layer and a correction term that is proportional to the real part of the elastic constant. The imaginary component can be shown to be due to the change in Δf_S. This means that rather than measure the impedance at resonance to determine the Q and hence the size of the viscous effect a complex version of the Sauerbrey equation can be defined which calculates the real and imaginary components of the mass spectra shown in equation 32. The complex Sauerbrey equation is

$$\mathbf{m}^*(f_{S2}) = m_0\frac{(f_{s1}+\Delta f_{s1}i)-(f_{s2}+\Delta f_{s2}i)}{(f_{s1}+\Delta f_{s1}i)} \tag{33}$$

where f_{S1} is the resonance frequency of the free quartz and f_{S2} is the resonance frequency of the quartz with the layer. The Δf_{S1} and Δf_{S2} are the half width at half max frequency values. It is interesting to note that if the imaginary component of the mass spectra is comparable to the real component then one needs to know something about the elastic properties of the layer in order to determine the correction term to the real part is small with respect to the mass m.

In order to investigate the sensitivity of equation 25 to changes in the parasitic impedance for the resonator before and after the layer is deposited a random error of the order of 0.1% was added to the real and imaginary components of the impedance of the resonator/layer composite. The error was seen to propagate to the spectra only in regions away from the resonance frequency of the piezoelectric with layer.

A systematic error in the form of a parallel capacitance on the input electrical terminals was also tested and the results are shown in Figure 9. The value of the parallel capacitance was adjusted from 10^{-1} to 10^{-5} of the clamped capacitance C_0 value of the resonator. As the size of the uncompensated parallel capacitance increases the curves move away from the theoretical curve except at f_s. An expanded view about the resonance frequency is shown in the inset, which suggests that the slope at f_s is unperturbed from the theoretical value. The transforms were applied to the two other cases shown in Figures 6 and 7 and as expected the curves replicate the theoretical acoustic impedance spectra of the layer. It should be noted that the determining the acoustic impedance spectra using the transform in equation 25 is not required since the spectra of the composite layer has an abundance of structure and in general the density and thickness of the layer can be determined independently. Acoustic loads in these regimes may be fit to the equation for the composite resonator using equation 7 and 20 as was done in previous work[22].

6. RESULTS

a) **Mass, Condensation, Evaporation and Curing studies using the QCM.**

In order to test the linear transform presented above polished Quartz AT cut crystals from Maxtek Inc. (P/N 149240-1 nominal 5MHz Ti/Pt electrodes) were mounted is the crystal holder after the holder was corrected for open and short parasitic impedances. The impedance spectrum of the unperturbed quartz crystal was then measured using an HP 4192a Impedance analyzer. The quartz and the holder were then immersed in distilled water and the impedance spectrum of the quartz crystal in contact with the water was measured. The results are shown in Figure 12. The material coefficients determined for the free quartz resonator are shown in Table 4. The impedance spectra for the free quartz resonator and the resonator immersed in distilled water is shown in Figure 10.

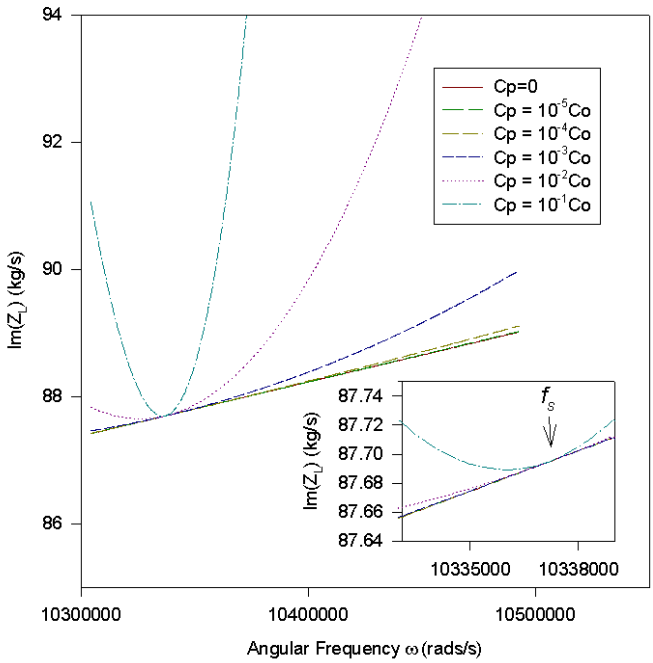

Figure 9 The imaginary part of the complex acoustic impedance spectra of the layer as a function of the angular frequency determine from the data in Figure 5. Each curve shown has a different uncompensated parallel capacitance added the spectra of the composite prior to the transfer shown in equation 25. The slopes of the various curves about f_s are seen to be equal in the inset figure. The resonance frequency is at 1.0337×10^7 rads/s.

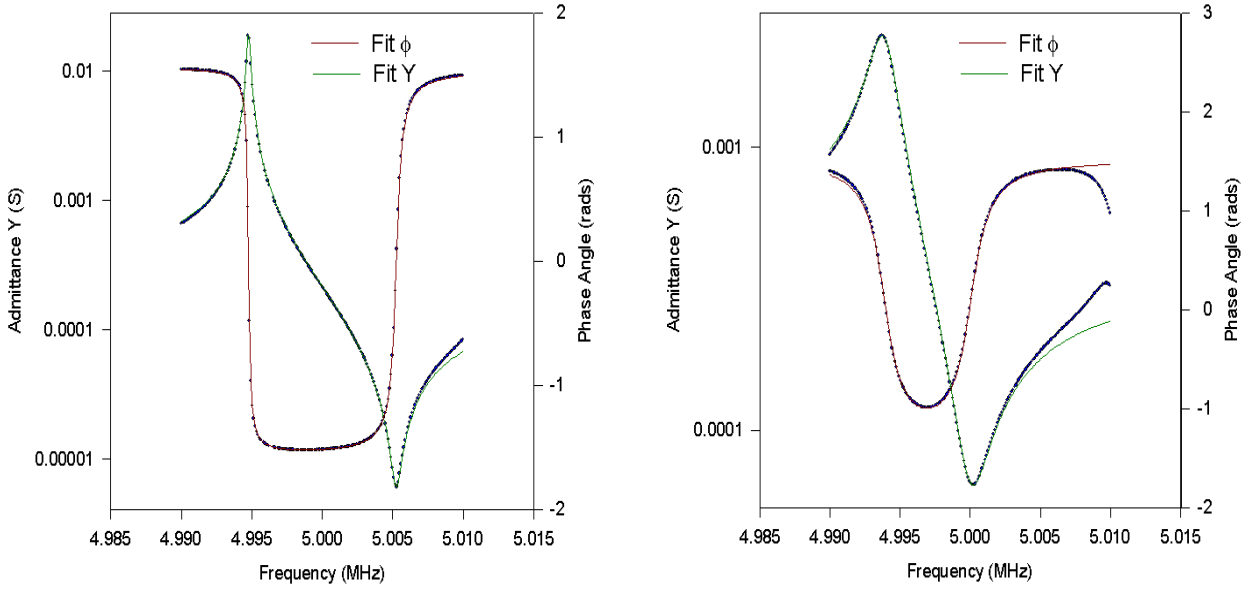

Figure 10. The admittance spectra of a 5 MHz Quartz crystal in air (left) and water (right) and the resultant fit using complex material coefficients. There is almost a ten-fold decrease in the quality of the resonance when immersed in water.

Table 4. The complex material coefficients from the spectra of the AT cut Quartz resonator in air show on the left in Figure 12. Material constants determined using Smits' method[15]. The complex resonance constants were determined from the resonance frequency and HWHM[24]

	AT Cut Quartz Resonator in air
$\boldsymbol{\varepsilon}^S$ (F/m)	$5.45933\text{x}10^{-11}(1 - 0.02388\text{i})$
$\mathbf{c}^D$ (N/m^2)	$2.94472\text{x}10^{10}(1 + 0.00012\text{i})$
$\boldsymbol{k}$ (#)	$0.0717744(1 - 0.00884\text{i})$
$\boldsymbol{h}$ (V/m)	$1.67\text{x}10^{9}(1 + 0.02084\ \text{i})$
ρ (kg/m^3)	2650
t (m)	0.000333
A (m^2)	$4.195\text{x}10^{-5}$
m_0 (kg)	$3.701\text{x}10^{-5}$
$\boldsymbol{f}_{sq}$ (Hz) (quartz)	$4.99477\text{x}10^{6} + 110.9\text{i}$
$\boldsymbol{f}_{s\,w}$ (Hz) (quartz + water)	$4.99390\text{x}10^{6} + 990.8\text{i}$
$\Delta\mathbf{m}$ (kg) (Sauerbrey eq.)	$6.45\text{x}10^{-9}\text{-}6.52\text{x}10^{-9}\text{i}$
$\Delta\mathbf{m}$ (kg) ($\mathbf{m}^*(\text{Re}(\boldsymbol{f}_{Sq}))$ Figure 11.	$6.44\text{x}10^{-9}\text{-}6.03\text{x}10^{-9}\text{i}$

The complex acoustic load $\mathbf{Z}_L(\omega)$ of the water and the effective mass spectra $\mathbf{m}^* = \mathbf{Z}_L(\omega)/i\omega$ of the water were determined using the transform (equation 25) , the coefficients in Table 4 and the two spectra in Figure 10. The complex mass spectrum is shown in Figure 11.

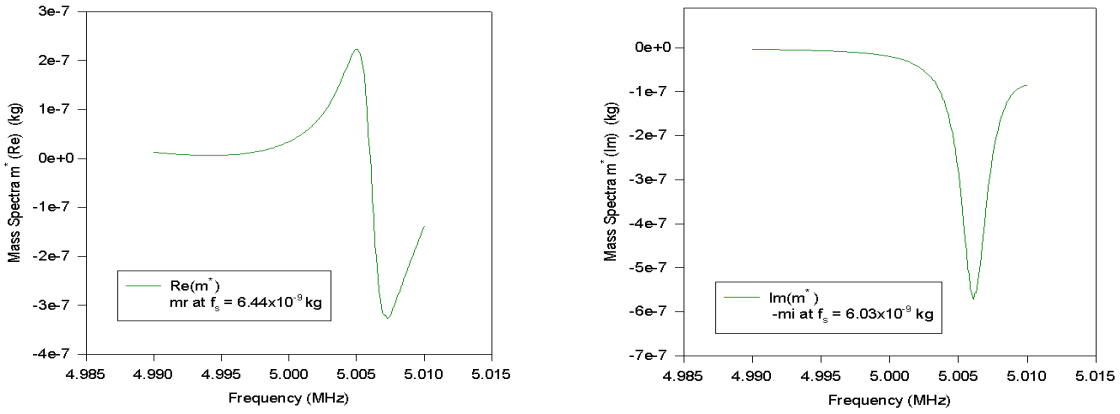

Figure 11. The complex effective mass spectra $\mathbf{m}^* = \mathbf{Z}_L(\omega)/i\omega$ determined for distilled water. The values of the complex mass determined at the series resonance frequency of the quartz in distilled water are shown in the figure.

The complex mass determined using the complex Sauerbrey equation (equation 33) with the complex series resonance frequencies of the quartz and the quartz in distilled water are shown in Table 4 along with the values determined from Figure 11. The values are found to be in good agreement.

In order to investigate the Quartz resonator as a monitoring device distilled water and epoxy were added to the surface of the resonator and the impedance spectra were measured as a function of time using a Solartron 1260 Analyzer. The results are shown in Figure 12. Abrupt jumps in the resonance frequency occur as the epoxy hardens and the water evaporates. When combined with a thermal chamber these resonators can also be used to measure dew points and possible freezing points of a variety of gas samples

.

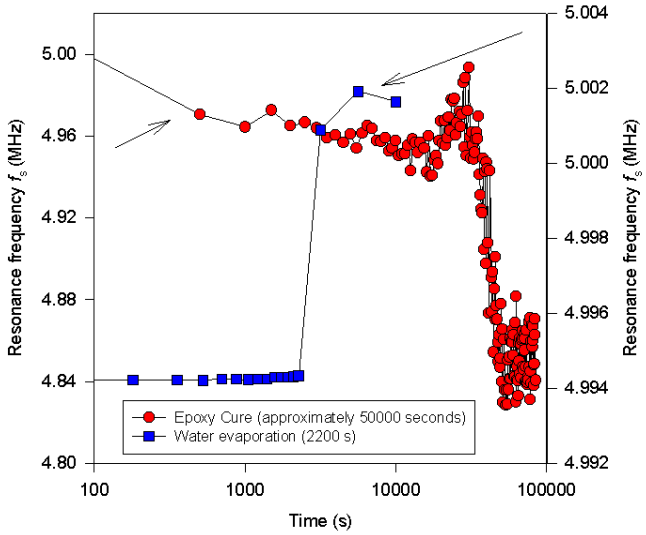

Figure 12. The room temperature series resonance frequency of the quartz with epoxy and water applied to the surface as a function of the time. The epoxy shows a physical change in loading at approximately 50000 seconds. The water evaporated from the crystal in 2200 seconds.

b) **Gauging layer elastic properties**

The impedance equation for the layer models shown in equations 7 and 20 were used to measure the longitudinal velocities and hence the elastic properties of polymer layers attached to piezoelectric PZT disks. The impedance of the disk was measured using a Solartron 1260 impedance analyzer prior to the layer attachment to determine starting values of the piezoelectric for the non-linear regression. A 70 micron layer of Kapton was coated with an epoxy (estimated to be less than 5 microns). The epoxy was reduced to a thin layer using a razor edge and the PZT disk was attached to the layer. The layer and disk were clamped and allowed to cure overnight. The impedance spectra of the PZT disk and the Kapton layer was then measured. The results are shown in Figure 13 below. The technique has been applied to Nafion layers however initial results suggest that the heavier electrode materials mass damp the resonance in the layers reducing the measured velocity. Tests are currently being prepared on samples of Nafion without electrodes.

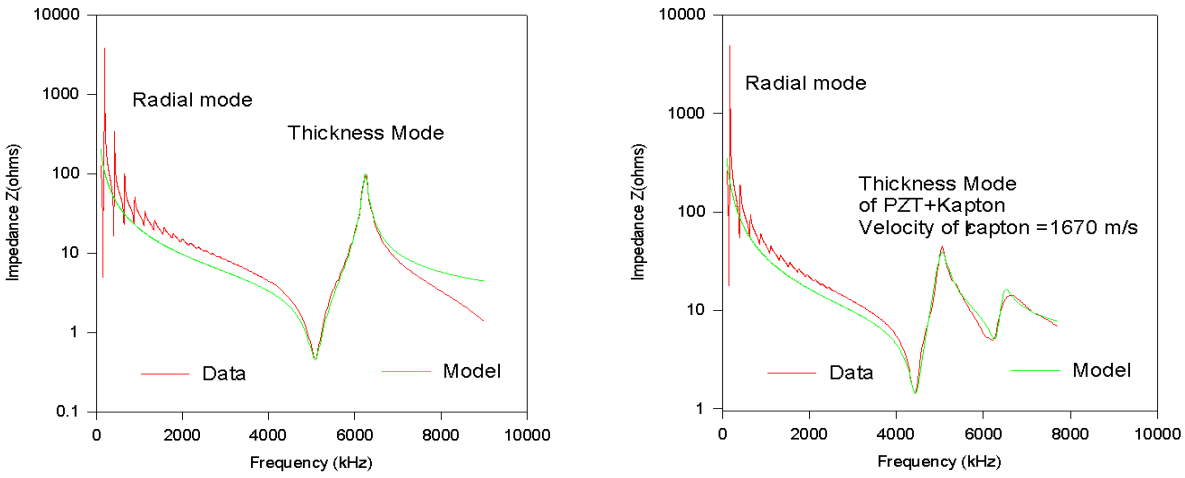

Figure 13. The impedance spectra of a PZT disk and a disk with a 70 micron Kapton layer. The longitudinal velocity of the layer was determined to be 1670 m/s

6. CONCLUSIONS

The solution to the piezoelectric with a layer based on Mason's transmission line model was presented with complex material coefficients. Three regimes were identified that were shown to load the transducer differently. These were the mass, elastic and radiation loading regimes. An alternative method based on a linear transform of the impedance data of the perturbed and unperturbed resonator was presented and a complex version of the Sauerbrey equation was presented which was found to be in agreement with the complex mass determined at the resonance frequency of the perturbed resonator. Examples using the quartz thickness shear resonators to monitor curing and evaporation were presented. The model was applied to PZT and Kapton composite resonator in the thickness mode and the longitudinal velocity of the Kapton was determined by relaxing the solution and fitting all the constants of the resonator.

ACKNOWLEDGEMENTS

The authors would like to thank Patricia Beauchamp for her support. The In Situ Exploration and Sample Return Center of Excellence at the Jet Propulsion Laboratory a division of the California Institute of Technology under a contract with the National Aeronautics Space Agency (NASA) and DARPA the Defense Advanced Projects Agency funded this research.

REFERENCES

[1] W..P. Mason, Electromechanical Transducers and Wave Filters, Princeton, NJ, Van Nostrand, 1948

[2] W.P. Mason, Physical Acoustics and the Properties of Solids, D. Van Nostrand Co., Princeton, NJ, 1958

[3] D. A. Berlincourt, D.R. Curran, H. Jaffe, "Chapter 3- Piezoelectric and Piezomagnetic Material and their Function in Transducers, pp. 169-270, Physical Acoustics-*Principles and Methods,* Volume 1-Part A, ed. W.P. Mason Academic Press, New York, 1964

[4] M. Redwood, "Transient Performance of a Piezoelectric Transducer", Journal of the Acoustical Society of America, **33**, pp.527-536, 1961

[5] S. Saitoh, H Honda, N. Kaneko, M. Izumi, S. Suzuki, The Method of Determining k_t and Q_m for low Q piezoelectric materials" Proceedings of the IEEE Symposium on Ultrasonics, San Francisco, CA, pp. 620-623, 1985

[6] Solid State Magnetic and Dielectric Devices, edited by H.W. Katz, John Wiley and Sons, New York , 1959

[7] R. Krimholtz, D.A. Leedom, G.L. Matthaei, "New Equivalent Circuit for Elementary Piezoelectric Transducers", Electron Letters, Electron. Lett. **6**, pp. 398-399,1970

[8] M. J. Zipparo, K.K. Shung, T.S. Shrout, "Piezoceramics for High Frequency (20-100 MHz) Single Element Imaging Transducers", IEEE Trans on Ultrasonics, Ferroelectrics and Frequency Control, **44**, pp.1038-1048, 1997

[9] F.S. Foster, L.K. Ryan, D.H. Turnbull, "Characterization of Lead Zirconate Titanate Ceramics for Use in Miniature High Frequency (20-80 MHz) Transducers, IEEE Trans on Ultrasonics, Ferroelectrics and Frequency Control , **38**, pp. 446-453, 1991

[10] Q. Zhang, P.A. Lewin, P.E. Bloomfield, "PVDF Transducers- A Performance Comparison of Single-Layer and Multilayer Structures", IEEE Trans on Ultrasonics, Ferroelectrics and Frequency Control, **44**, pp.1148-1156, 1997

[11] R.L. Goldberg, M.J. Jurgens, D.M. Mills, C.S. Henriquez, D.Vaughan, S. W. Smith, "Modeling of Piezoelectric Multilayer Ceramics Using Finite Element Analysis", IEEE Trans on Ultrasonics, Ferroelectrics and Frequency Control., **44**, pp. 1204-1214, 1997

[12] Sherrit S., S. P. Leary, and Y. Bar-Cohen "Comparison of the Mason and KLM Equivalent Circuits for Piezoelectric Resonators in the Thickness Mode," Proceedings of the IEEE International Ultrasonics Symposium, held in Lake Tahoe, CA, 17-20 October 1999b.

[13] IEEE Standard on Piezoelectricity, IEEE/ANSI Std. 176-1987

[14] S. Sherrit and B.K. Mukherjee, "The Use of Complex Coefficients to Model Piezoelectric Materials", Proceedings of the IEEE Symposium on Ultrasonics, pp. 633-640, Sendai Japan, 1998

[15] J.G. Smits, "Iterative Method for Accurate Determination of the Real and Imaginary Parts of Materials Coefficients of Piezoelectric Ceramics", IEEE Trans on Sonics and Ultrasonics, (**SU-23**), (6), pp. 393-402, November, 1976

[16] J.G. Smits, "High Accuracy Determination of Real and Imaginary Parts of Elastic, Piezoelectric, and Dielectric Constants of Ferroelectric PLZT (11/55/45) Ceramics with Iterative Method", Ferroelectrics, **64**, pp.275-291, 1985

[17] S.Sherrit, H.D. Wiederick, B.K. Mukherjee, "A Non-Iterative Method to Determine the Real and Imaginary Material Constants of a Piezoelectric Material", Ferroelectrics, **134**, pp. 111-119, 1992

[18] S. Sherrit, N. Gauthier, H.D. Wiederick, B.K. Mukherjee , "Accurate Evaluation of the Real and Imaginary Material Constants of a Piezoelectric Resonator in the Radial Mode"., Ferroelectrics, **119**, pp. 17-32, 1991

[19] W.P. Mason, “Physical Acoustics and the Properties of Solids”, Princeton, D. Van Nostrand Co. Inc., 1958

[20] H.J. McSkimmin , “Chapter 4- Ultrasonic Methods for Measuring the Mechanical Properties of Liquids and Solids, pp. 271-334, Physical Acoustics-*Principles and Methods,* Volume 1-Part A, ed. W.P. Mason Academic Press, New York, 1964

[21] Kenneth M. Lakin, Gerald R. Kline, Kevin T. McCarron, "High Q Microwave Acoustic Resonators and Filters" IEEE Trans. On Microwave Theory and Techniques, **41**, pp. 2139-2146, 1993

[22] M. Lukacs, T. Olding, M. Sayer, R. Tasker, S. Sherrit, "Thickness mode material constants of a supported piezoelectric film", J. of Applied Physics , **85**, pp.2835-2843, 1999

[23] G. Sauerbrey, “Verwendung von Schwingquarzen sur Wägung Dünner Schichten und zur Mikrowägung –*Translation - Use of vibrating quartz for weighing of thin layers and for micro weighing*”, Z. Physik, **155**, pp. 206-222, 1959

[24] S. Sherrit, H.D. Wiederick, B.K. Mukherjee, M. Sayer, "An Accurate Equivalent Circuit for the Unloaded Piezoelectric Vibrator" , J. Physics D. (Applied Physics), **30**, pp 2354 - 2363, 1997

[25] A. Arnau, T. Sogorb, Y. Jimenez, “ A New Method for Continuous Monitoring the Series Resonance Frequency and Simple Determination of Motional Impedance Parameters for Unloaded Quartz Crystal Resonators” IEEE Trans. on Ultrasonics, Ferroelectrics and Frequency Control, **48**, 2, pp. 617-623, March 2001

[26] R.W. Cernosek, S.J. Martin, A.R. Hillman, H.L Bandy, “Comparison of the Lumped-Element and Transmission-Line models for the Thickness-Shear-Mode Quartz Resonator Sensors, IEEE Trans. on Ultrasonics, Ferroelectrics and Frequency Control, **45**, 5, pp. 1399-1407, Sept.,1998

[27] S.S. Narine, A.J. Slavin, “Use of the quartz crystal microbalance to measure the mass of submonolayer deposits: Measuring the stoichiometry of surface oxides” J. Vac. Sci. Technol. A 16 (3), pp. 1857-1862, May/June 1998